ELSEVIER

Atmospheric Research 83 (2007) 254–262

ATMOSPHERIC RESEARCH

www.elsevier.com/locate/atmos

The thermodynamic structure atop a penetrating convective thunderstorm

Pao K. Wang

Department of Atmospheric and Oceanic Sciences, University of Wisconsin-Madison, 1225 W. Dayton St., Madison, WI 53706, USA

Accepted 7 August 2005

Abstract

The thermodynamic structure on top of a numerically simulated severe storm is examined to explain the satellite observed plume formation above thunderstorm anvils. The same mechanism also explains the formation of jumping cirrus observed by Fujita on board of a research aircraft. A three-dimensional, non-hydrostatic cloud model is used to perform numerical simulation of a supercell that occurred in Montana in 1981. Analysis of the model results shows that both the plume and the jumping cirrus phenomena are produced by the high instability and breaking of the gravity waves excited by the strong convection inside the storm. These mechanisms dramatically enhance the turbulent diffusion process and cause some moisture to detach from the storm cloud and jump into the stratosphere. The thermodynamic structure in terms of the potential temperature isotherms above the simulated thunderstorm is examined to reveal the instability and wave breaking structure. The plumes and jumping cirrus phenomena represent an irreversible transport mechanism of materials from the troposphere to the stratosphere that may have global climatic implications.

Keywords: Plumes; Thunderstorms; Gravity waves; Wave breaking; Stratospheric water vapor; Stratosphere–troposphere exchange

1. Background

Recently, the phenomenon of penetrating convective storms has received some attention because of its potential implications on the transport of various chemical species from the troposphere into the stratosphere. This phenomenon was first mentioned in the 1980s (e.g., Negri, 1982; Adler and Mack, 1986), but was clearly identified only in the 1990s (Setvak and Doswell, 1991; Levizzani and Setvàk, 1996). The main feature of the penetrating convection in these observational studies is the chimney-plume-like cirrus clouds above the thunderstorm anvils. We will call these cirrus clouds the *cirrus plume* hereafter. Fig. 1 shows an example of such plume cirrus. In some cases, the vertical distance between the anvil and the cirrus plume can be estimated and one example shows a vertical distance of ~3 km (Levizzani and Setvàk, 1996). Since the storms exhibiting the cirrus plume phenomenon are usually severe, their anvils are generally at the tropopause level. Hence, the fact that plumes are higher than the anvils implies that they are well within the lower stratosphere.

Wang (2003) provided the physical interpretation of this phenomenon. He used a 3-D nonhydrostatic cloud model to perform simulation of a severe thunderstorm and analyzed the results to show that the cirrus plumes occurred in the simulated storm and their properties

E-mail address: pao@windy.aos.wisc.edu.

0169-8095/$ - see front matter © 2006 Elsevier B.V. All rights reserved.
doi:10.1016/j.atmosres.2005.08.010

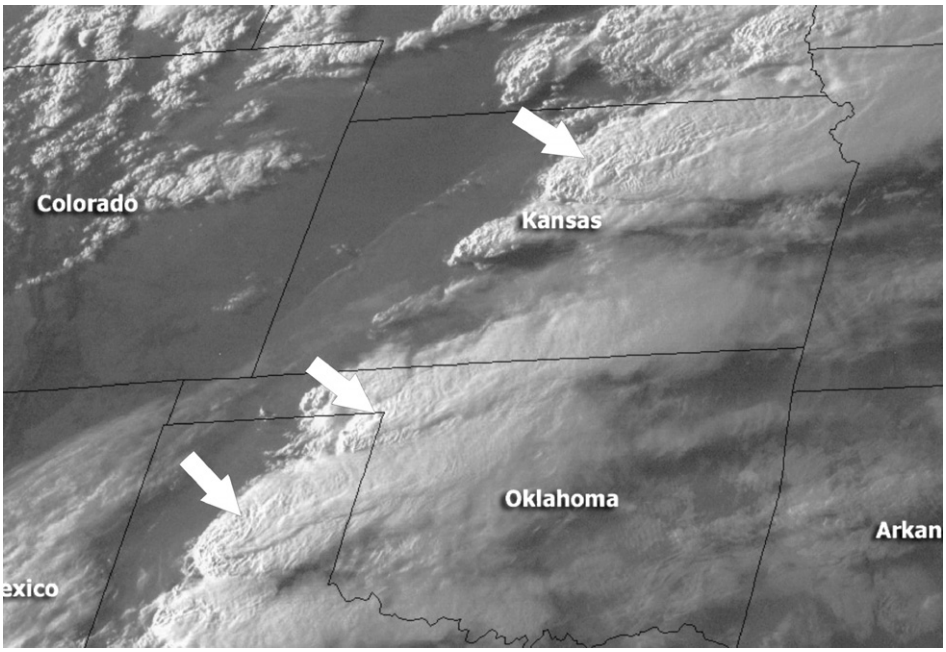

Fig. 1. GOES-8 composite channels 1, 3 and 4 imagery of 0015 UTC, 06 May 2002 in the Plains of US showing a row of thunderstorms with anvil top plumes (indicated by white arrows) (courtesy of NOAA).

resemble closely to the major characteristics of that observed by satellites (Levizzani and Setvàk, 1996). By a vertical cross-sectional analysis of the same simulated storm, Wang (2004) showed that the *cirrus plumes* arising from the anvil-sheet correspond to the jumping cirrus as observed by Fujita (1982, 1989).

A major point of Wang (2003, 2004) is that both cirrus plumes and jumping cirrus are produced by the gravity wave breaking on the cloud top of the storm. It is well known that severe storms excite gravity waves (e.g., Fovell et al., 1992; Alexander et al., 1995; Lane et al., 2001, 2003). Under sufficient unstable conditions, wave breaking can occur that may result in part of the storm, especially the cloud top, becoming detached and ejected upward into the lower stratosphere (Wang, 2003). The wave breaking process represents an irreversible, non-adiabatic mass transfer from the troposphere to the stratosphere. In Wang (2003, 2004), the gravity wave breaking phenomenon was shown by using a single vertical cross-sectional slice of the relative humidity profile overlaid with potential temperature isotherms. No detailed analysis was given as far as the wave breaking process is concerned. Also, the wave breaking process on the overshooting top has not been discussed. In view of the potential significance of this process to the stratosphere–troposphere exchange, it is useful to give a more detailed analysis of the cloud top processes so as to reveal the thermodynamics and dynamics of this phenomenon. This paper is motivated by this need.

2. The cloud model and the CCOPE supercell

The tool utilized for the present study is the Wisconsin Dynamical/Microphysical Model (WISC-DYMM), which is a three-dimensional, quasi-compressible, time-dependent, non-hydrostatic primitive-equation cloud model developed at the University of Wisconsin-Madison by the author's research group. This model has been used in several earlier studies and some details of it have been reported before (see, for example, Johnson et al., 1993, 1995; Wang, 2003), hence will not be repeated here.

The storm chosen for the simulation for illustrating the plume-formation mechanism is a supercell that passed through the center of the Cooperative Convective Precipitation Experiment (CCOPE) observational network in southeastern Montana on 2 August 1981. The storm and its environment were intensively observed for more than 5 h by a combination of seven Doppler radars, seven research aircraft, six rawinsonde stations and 123 surface recording stations as it moved east–southeastward across the CCOPE network. Again, the observational history of this storm has been reported previously (Miller et al., 1988; Wade, 1982) and readers are referred to these sources for further details. The

storm has also been successfully simulated using WISCDYMM and the general dynamical and microphysical behaviors were reported by Johnson et al. (1993, 1995). The current study uses the simulated CCOPE storm that was initialized by the same conditions as in Johnson et al. (1993, 1995), but with finer resolution, i.e., $1\times1\times0.2$ km^3. This is the same as that analyzed in Wang (2003).

3. Results and discussion

The simulated storm exhibits two different modes of cirrus plume formation, one occurred at $t=20$–30 min into the simulation in the downstream anvil-sheet region; the other occurred several times, but the major one occurred at $t=70$–80 min in the overshooting dome (Wang, 2003). The first mode seems to correspond most closely with the jumping cirrus reported by Fujita and the second mode corresponds closely to the satellite-observed cirrus plumes. They will be described separately in the following subsections.

3.1. Anvil-sheet cirrus plume (20–30 min)

Fig. 2 shows three snapshots of the plume formation during the 20–30 min into the simulation. Fig. 2(A) shows the RHi (relative humidity with respect to ice) distribution overlaid with the potential temperature (θ) isotherms in the central west–east cross-section ($y=27$ km) of the simulated storm at $t=20$ min. This cross-section is usually (though not always) where the storm updraft is the maximum in the computational domain and will be used to represent the storm activity center in this study. Note that only the upper portion of the cross-section ($z=10$–20 km) is shown, as the lower portion of the storm is not important to the current study. Note also that the θ-isotherms above 400 K have a different interval than those below, as explained in the figure legend. Even at this stage, the gravity waves have already been developed, as can be seen from the wavy nature of the θ-isotherms and the velocity vectors. The gravity wave "trough" extends from the cloud top ($x\sim40$ km, $z\sim11.5$ km) upward and tilts westward to $z\sim17$ km.

At this early stage of the storm life, the updrafts have just pushed the overshooting dome above the tropopause at $z\sim12.5$ km (Johnson et al., 1995) to just slightly below 13 km. Two θ-isotherms (375 K and 385 K) exhibit wave breaking characteristics right above the dome and causing small amount of moisture to be ejected from the cloud, but the amount is insignificant. On the other hand, the θ-isotherms above the downstream cloud top bulge up prominently that eventually lead to wave breaking.

The potential temperature field in this situation is very much like large-scale flow past a mountain such as the Rockies in western US where the instability developed in the lee side of the mountain (see, for example, Baines, 1995). In the present case, the strong updrafts induced by the deep convection serve to block the ambient flow, thus behave as a mountain-like obstacle and generate such instability.

Fig. 2(B) shows the same cross-section at $t=1570$ s. The wave breaking is imminent as can be seen from the kink of the 385 K θ-isotherm right above the cloud top. The overshooting dome actually lowers somewhat at this time, from $z\sim13$ km to $z\sim12.5$ km, a drop of about 500 m. The wave crest at the cloud top, which was at $x\sim42$ km in Fig. 2(A), now moves westward to $x\sim38$ km and its amplitude is greatly amplified. A third wave crest located at $x\sim48$ km is also visible.

The main wave breaking event occurs above the second wave crest. Here a large patch of moisture in form of a surge is detached from the cloud top and protrudes into the stratosphere above to about 15.5 km. The motion is mainly in the direction perpendicular to the isotherms and hence is highly diabatic. The vertical distance between the highest and lowest points of 380 K isotherm is only slightly less than 2 km. The deepening of the wave trough is obvious compared to that in Fig. 2(A).

Note that the wave breaking occurs a moment after the lowering of the overshooting dome, a sequence exactly corresponding to the statement of Fujita (1982) that "One of the most striking features seen repeatedly above the anvil top is the formation of cirrus cloud which jumps upward from behind the overshooting dome as it collapses violently into the anvil cloud". Wang (2004) used this statement to identify the wave breaking as the mechanism for the jumping cirrus.

Fig. 2(C) shows the same central cross-section but at $t=1800$ s. The three-crest cloud top structure is even more prominent than in Fig. 2(B). The wave breaking signature of the 380 K isotherm is unmistakable and the region becomes highly turbulent. Two 'rotors' form in this region: one centers just below the crest of 385 K isotherm, while the other centers just above the valley point of 380 K isotherm. The moisture patch (plume) associated with the upper rotor is almost detached from the source below, which seems to resemble the water drops detached from a breaking ocean wave. Furthermore, the wave motion at third crest also pushes a large patch of moisture upward and upstream. These plumes eventually separated themselves from the cloud and moved downstream.

Throughout the 3-h simulation, the anvil-sheet plume only occurred once and seems to be closely associated with substantial changes of the overshooting dome; the latter is also related to the jumping cirrus as described by Fujita (1982, 1989). It is believed that the wave breaking at this stage is caused by the buildup of a critical layer near the cloud top due to the deep convection, just like the case examined by Lane et al.

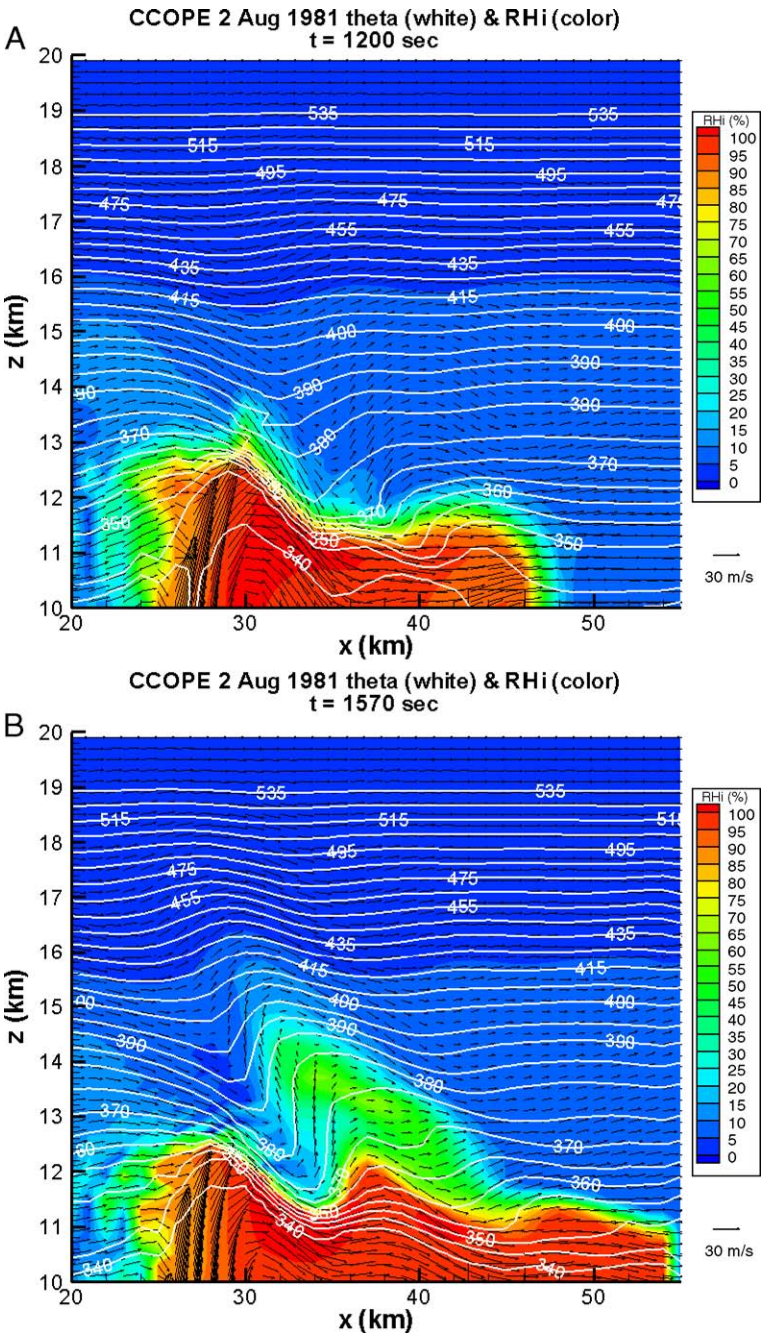

Fig. 2. (A) Snapshot of the RHi profile (color) overlaid with potential temperature isotherms (white) in the central west–east cross-section (y=27 km) of the simulated CCOPE storm at t=1200 s. Black arrows represent wind velocity. Note that the wind vectors below the cloud top are stacked together due to the relatively large magnitudes (typically greater than 40 m s^{-1}). Note also that the potential temperature isotherm (isentrope) immediately above 400 K is 405 K; the subsequent isotherms are 415 K, 425 K, 435 K, etc. This is done to prevent the crowding together of those isotherms in the higher level. (B) Same as (A) except for t=1570 s. (C) Same as (A) except for t=1800 s.

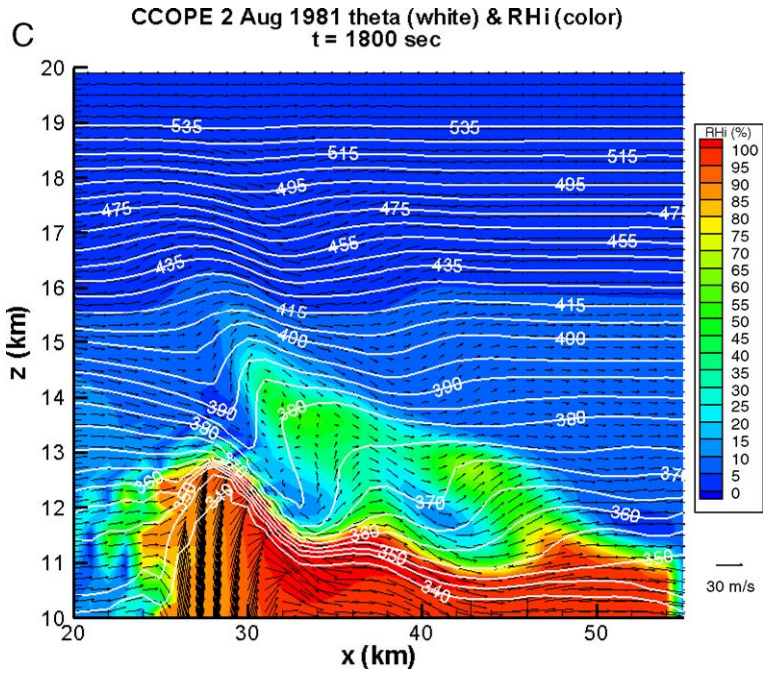

Fig. 2 (*continued*).

(2003). A detailed analysis on the 3-D internal gravity wave structure of this case is being conducted in order to ascertain this point and the results will be reported in the near future.

If we use the RHi=30% contour to represent the wave surface and trace the motion of its front edge during the breaking, we can estimate the velocity of the moisture ejection due to this mechanism. Fig. 3 shows the results where the *x*- and *y*-coordinates of the front edge as a function of time. The slope of the curves determines the *x*- and *z*-components (*u*, *w*) of the velocity. The maximum magnitude of *u* and *w* estimated from these curves are 28 and 15 m s^{-1}, respectively.

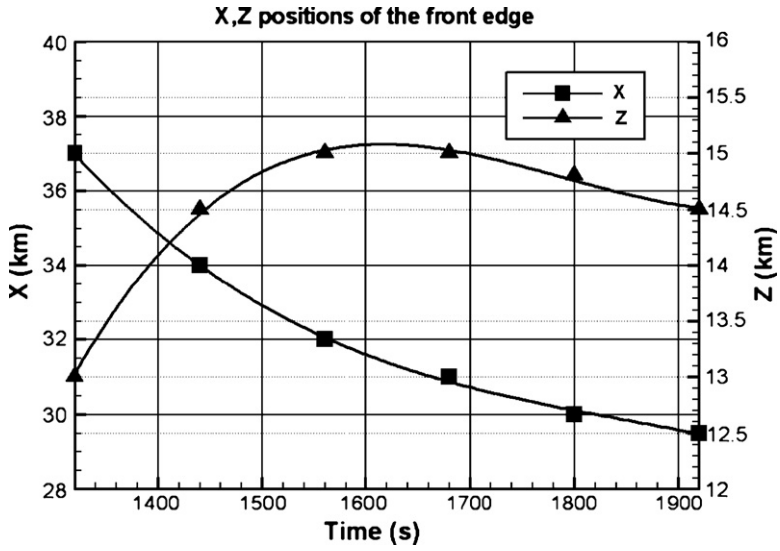

Fig. 3. The *x*, *z* positions of the front edge of the RHi=30% region in the central west–east cross-section as a function of time from *t*=1320 s to 1920 s.

3.2. Overshooting cirrus plumes (70–80 min)

The other mode of cirrus plume formation occurs several times in the simulation but a major one occurs in 70–80 min into the simulation. As in Wang (2003), we shall call plumes formed this way as the overshooting cirrus plumes. Unlike the previous stage when the overshooting dome was not fully developed, the dome seems to be in a quasi-steady state at this time. The plumes produced in this stage appear to be a result of small-scale wave breaking near the dome.

Fig. 4(A) shows again the central west–east cross-section as in Fig. 2(A) but at $t=4200$ s. The overshooting dome reaches an altitude of ~15 km, nearly

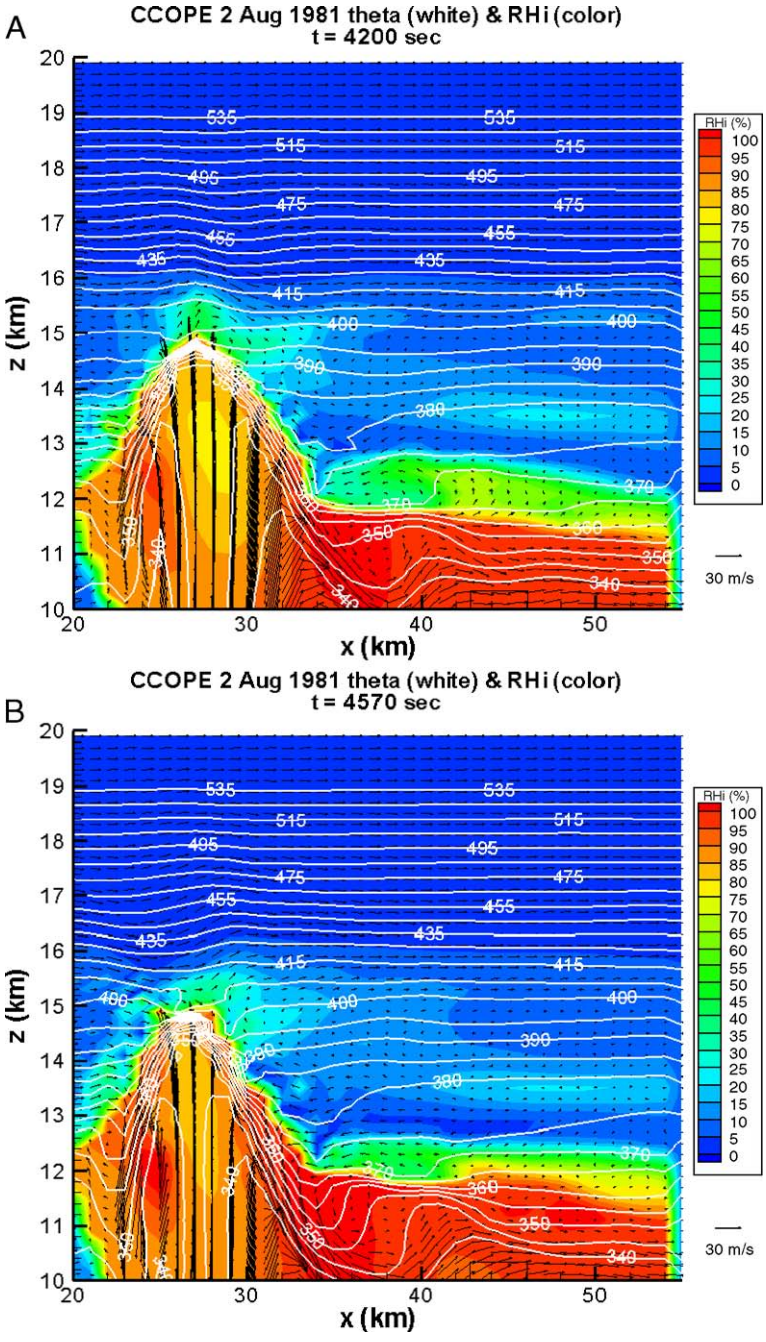

Fig. 4. (A) Same as Fig. 2(A) except for $t=4200$ s. (B) Same as Fig. 2(A) except for $t=4570$ s. (C) Same as Fig. 2(A) except for $t=4800$ s.

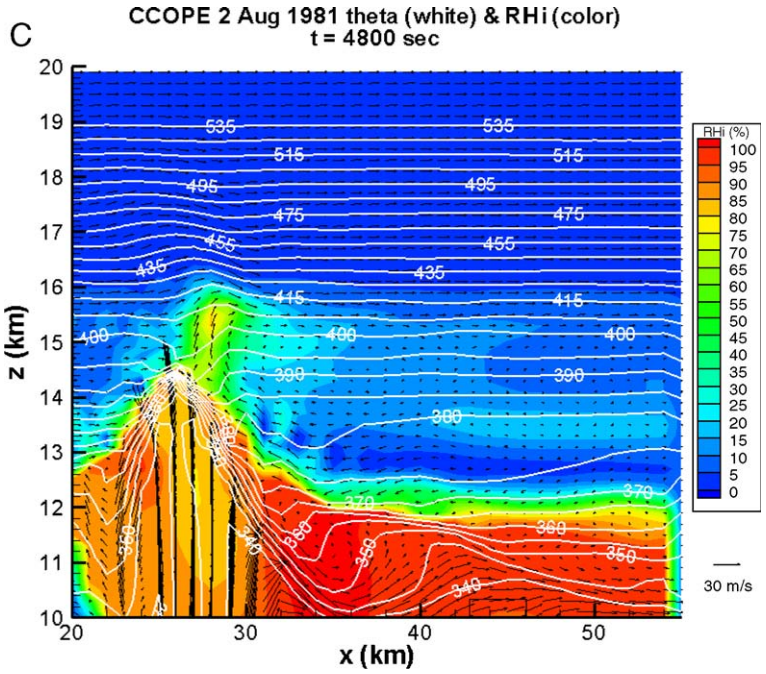

Fig. 4 (*continued*).

2.5 km higher than the pre-storm tropopause. The dome is characterized by a cold and dry core and very large θ-gradients in the dome shell. The normal potential temperature gradient $\partial\theta/\partial n$ where n is the distance outward and normal to the dome surface is on the order of 0.12 K m^{-1} (or 120 K km^{-1}). The wind vectors are mostly vertical inside the dome and the speeds are normally greater than 40 m s^{-1} at this stage. There are large areas of neutrally stratified air inside the dome, but this is not the focus of this paper. Above the dome, the air is largely stably stratified at this stage except the 380 K isotherm at $x \sim 36$ km.

Immediately outside the dome, the wind speeds are small and the directions change rapidly. Thus, the wind shear near the dome shell is very large and turbulence can be generated easily. Small area of moisture ejection is seen right on top of the dome due to a previous instability.

Note also that the wind field above the anvil-sheet region is much more complicated than that in the previous stage. In Fig. 2(A)–(C), the winds in this region were westerly and of fairly large speed ($\sim$30 m s^{-1}). In this stage, the winds are weaker but the directions are quite non-uniform. Many eddies of the scale $\sim$10 km are present in this region and inside the anvil as well.

Fig. 4(B) shows the same cross-section at t=4570 s. Now the 405 K isotherm exhibits clear wave breaking signature and moisture is being ejected from this region. Other isotherms such as 390 K and 400 K also show near wave breaking signatures. Immediately above the anvil downstream of the dome the winds are easterly and generally converge with the westerly winds at the top of the dome.

Fig. 4(C) shows the same cross-section at t=4800 s. The moisture patch is largely disconnected with the cloud below at this time and is carried by the higher level westerlies to the downstream, eventually forming the chimney plume feature as observed by satellites (Levizzani and Setvàk, 1996). The plume is roughly 3 km above the general anvil deck, again consistent with the satellite observation.

As mentioned above, unlike the anvil-sheet plumes, which occurred only once, the overshooting plumes occurred many times throughout the 3-h simulation. Although the most prominent plumes seem to originate right at the top of the overshooting dome, there are other locations, such as the downwind slope of the dome, where instabilities occurred and plumes formed. Thus, overshooting plumes may have more than one layer structure and there may be more than one overshooting plume at a given instant. Fig. 5 shows a possible candidate of such multilayer plumes on top of a tornadic storm occurred in northern Wisconsin. This point may have some significance for the identification of plumes using satellite imageries.

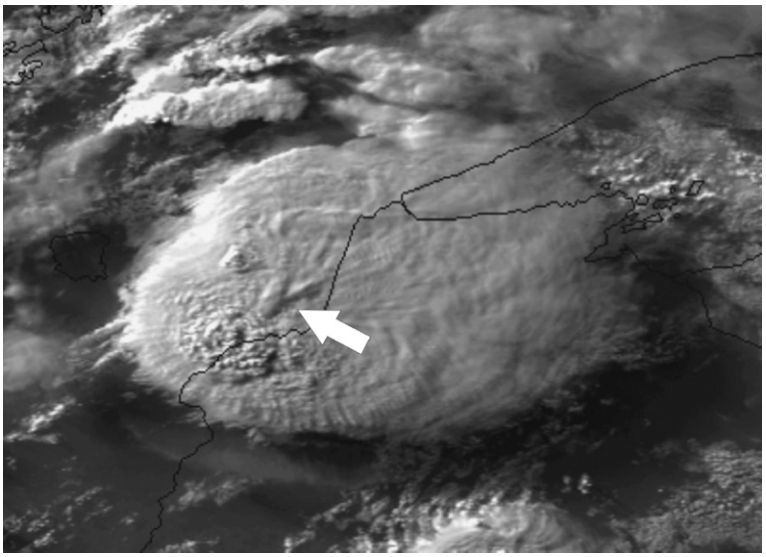

Fig. 5. NOAA-15 AVHRR visible imagery of the tornadic storm in northern Wisconsin at 0059 UTC, 19 June 2001. The white arrow indicates possible double plume feature on the storm top (courtesy of NOAA).

3.3. Wave breaking mechanism

The above discussions established that both kinds of cirrus plumes are produced by gravity wave breaking at the cloud top which results in moisture being injected into the stratosphere from the cloud body. As to the mechanisms responsible for gravity wave breaking in a thunderstorm, our knowledge is still limited and more studies need to be performed. Recent study performed by Lane et al. (2003) should shed some lights on this topic. Lane et al. (2003) performed high resolution two- and three-dimensional numerical simulations on the turbulence generation above a developing thunderstorm near Dickinson, North Dakota on 10 July 1997. Their three-dimensional simulation results did not show wave breaking, but the two-dimensional results did. From their analysis of the two-dimensional results, they concluded that the wave breaking is due to the building up of a critical layer near the layer of neutral buoyancy (LNB). Fovell et al. (1992) showed that a severe storm generates gravity waves by the mechanical oscillation of convective updrafts about their LNB; hence, the intrinsic gravity wave frequency should be equal to the local Brunt-Väisälä frequency. Once the local wind speed relative to the storm becomes the same as the speed of the gravity wave, a critical layer is build up. At this time, the only way to dissipate wave energy is via wave breaking. They thus concluded that the wave breaking is due to the building up of a local critical layer by the deep convection. They indicated that the wind speed at LNB relative to the storm in their three-dimensional results never reached the critical level and hence no wave breaking occurred.

The present study is a three-dimensional case and the spectral analysis is more involved. We are performing such analysis and hope to publish the results in the future.

4. Conclusions

A 3-D, nonhydrostatic cloud model is used to simulate a severe thunderstorm occurred in midwest US and the results are used to illustrate the cirrus plume formation process. Two different modes of storm top plume formation are examined and both are shown to associate with the cloud top gravity wave breaking. Such gravity wave motions are commonly observed on top of severe thunderstorms and there are many examples of such phenomenon in satellite thunderstorm imageries. The first mode, the anvil-sheet cirrus plume is identified as the mechanism producing the jumping cirrus reported by Fujita (1982, 1989). The second mode, the overshooting cirrus plume, is identified as the mechanism of the chimney plume feature observed by Levizzani and Setvàk (1996) and Setvak and Doswell (1991).

Wang (2003) showed that the plumes transport moisture from the troposphere to the stratosphere and the rate for this particular storm is $\sim$3 tons s^{-1}. It is unclear at present whether this number is an over-estimate or underestimate and whether other storms of similar severity would transport similar amount of

moisture to the stratosphere. There is a need to ascertain the significance of this transport process because water vapor is an important infrared absorber in the atmosphere and their wide distribution in the stratosphere may have important impact on the global climate (see, e.g., Liou, 2002).

Acknowledgments

This research is supported by NSF grants ATM-0234744 and ATM-0244505 and NOAA GIMPAP grant to the University of Wisconsin-Madison.

References

Adler, R.F., Mack, R.A., 1986. Thunderstorm cloud top dynamics as inferred from satellite observations and a cloud top parcel model. J. Atmos. Sci. 43, 1945–1960.

Alexander, M.J., Holton, J.R., Durran, D.R., 1995. The gravity wave response above deep convection in a squall line simulation. J. Atmos. Sci. 52, 2212–2226.

Baines, P.G., 1995. Topographic Effects in Stratified Flow. Cambridge University Press. 482 pp.

Fovell, R., Durran, D., Holton, J.R., 1992. Numerical simulation of convectively generated stratospheric gravity waves. J. Atmos. Sci. 49, 1427–1442.

Fujita, T.T., 1982. Principle of stereographic height computations and their application to stratospheric cirrus over severe thunderstorms. J. Meteorol. Soc. Jpn. 60, 355–368.

Fujita, T.T., 1989. The Teton-Yellowstone tornado of 21 July 1987. Mon. Weather Rev. 117, 1913–1940.

Johnson, D.E., Wang, P.K., Straka, J.M., 1993. Numerical simulation of the 2 August 1981 CCOPE supercell storm with and without ice microphysics. J. Appl. Meteorol. 32, 745–759.

Johnson, D.E., Wang, P.K., Straka, J.M., 1995. A study of microphysical processes in the 2 August 1981 CCOPE supercell storm. Atmos. Res. 33, 93–123.

Lane, T.P., Reeder, M.J., Clark, T.L., 2001. Numerical modeling of gravity wave generation by deep tropical convection. J. Atmos. Sci. 58, 1249–1321.

Lane, T.P., Sharman, R.D., Clark, T.L., Hsu, H.-M., 2003. An investigation of turbulence generation mechanisms above deep convection. J. Atmos. Sci. 60, 1297–1321.

Levizzani, V., Setvàk, M., 1996. Multispectral, high resolution satellite observations of plumes on top of convective storms. J. Atmos. Sci. 53, 361–369.

Liou, Kuo-Nan, 2002. An Introduction to Atmospheric Radiation, 2nd edition. Academic Press. 582 pp.

Miller, L.J., Tuttle, D., Knight, C.A., 1988. Airflow and hail growth in a severe northern High Plains supercell. J. Atmos. Sci. 45, 736–762.

Negri, A.J., 1982. Cloud-top structure of tornado storms on 10 April 1979 from rapid scan and stereo satellite observations. Bull. Am. Meteorol. Soc. 63 (10), 1151–1859.

Setvak, M., Doswell III, C.A., 1991. The AVHRR channel 3 cloud top reflectivity of convective storms. Mon. Weather Rev. 119, 841–847.

Wade, C.G., 1982. A preliminary study of an intense thunderstorm which moves across the CCOPE research network in southeastern Montana. Proc. Ninth Conf. on Weather Forecasting and Analysis. Amer. Meteor. Soc., Seattle, WA, pp. 388–395.

Wang, P.K., 2003. Moisture plumes above thunderstorm anvils and their contributions to cross tropopause transport of water vapor in midlatitudes. J. Geophys. Res. 108 (D6), 4194, doi:10.1029/2003JD002581.

Wang, P.K., 2004. A cloud model interpretation of jumping cirrus above storm top. Geophys. Res. Lett. 31, L18106, doi:10.1029/2004GL020787.